Journal of Materials Chemistry C

PAPER

View Article Online
View Journal | View Issue

Cite this: J. Mater. Chem. C, 2014, 2, 542

Superhydrophobic surface enhanced Raman scattering sensing using Janus particle arrays realized by site-specific electrochemical growth†

Shikuan Yang,*[a] Patrick John Hricko,[a] Po-Hsun Huang,[a] Sixing Li,[a] Yanhui Zhao,[a] Yuliang Xie,[a] Feng Guo,[a] Lin Wang[b] and Tony Jun Huang*[a]

Received 19th August 2013
Accepted 21st October 2013

DOI: 10.1039/c3tc31635a

www.rsc.org/MaterialsC

Site-specific electrochemical deposition is used to prepare polystyrene (PS)–Ag Janus particle arrays with superhydrophobic properties. Analyte molecules can be significantly enriched using the superhydrophobic properties of the PS–Ag Janus particle array before SERS detection, enabling the extremely sensitive detection of molecules in a highly diluted solution (*e.g.*, femtomolar level). The superhydrophobic surface enhanced Raman scattering sensing concept described here is of critical significance in biosensing and bioanalysis. Most importantly, the site-specific electrochemical growth method we developed here is a versatile approach that can be used to prepare Janus particle arrays with different properties for various applications.

1 Introduction

Low-concentration detection of biological species is critical for medical and biological applications.[1] For instance, low-concentration biomarker and antigen detections could improve early-stage identification of diseases (*e.g.*, cancer), where early detection is exceptionally important for the survival of patients.[2–4] Surface enhanced Raman scattering (SERS) is an extensively studied method for low-concentration detection because of its unique benefits including being label-free, highly specific, and having sensitive sensing capabilities.[5–11] In order to further increase SERS sensitivity, various "top down" and "bottom up" fabrication techniques have been developed to generate SERS substrates integrated with numerous "hot spots" (*i.e.*, SERS sensitive sites).[8–11] However, it is challenging to significantly enhance SERS sensitivity by solely optimizing the structure of the SERS substrates. Therefore, new concepts capable of further augmenting the SERS sensitivity are highly desirable.

Surface wetting properties are important in anti-fogging, self-cleaning, and oil/water separation fields.[12–15] Both surface modification and surface microstructure design can adjust surface wetting behaviors.[12–15] For example, a hydrophobic surface usually becomes more hydrophobic upon increasing its surface roughness.[12,13] Coincidentally, roughness also plays an important role in improving SERS performance.[5–8] This fact inspired us to combine the superhydrophobic surface design and SERS substrate design together by preparing highly surface-roughened noble metal nanostructure arrays. The designed SERS substrate with a superhydrophobic surface is used first to greatly concentrate molecules by several million-fold in a highly diluted solution (*e.g.*, initially femtomolar level), and then drive the concentrated sample into a localized area bearing dense "hot spots" to be probed by SERS. This superhydrophobic surface enhanced Raman scattering (SSERS) concept opens a new avenue towards significantly augmenting the SERS sensitivity without the need for complex procedures to optimize the substrate structure. The SSERS substrate could find applications in the areas of ultrasensitive biosensing and environmental pollution monitoring. Here, site-specific electrochemical deposition (ED) was used to prepare micro/nano-structured polystyrene (PS)–Ag Janus particle arrays with superhydrophobic surfaces. It is noteworthy to mention that the site-specific ED growth concept greatly expands ED capabilities in fabricating nanomaterials with well-defined structures, which can be immediately extended into other material systems (*e.g.*, Cu, Pt, MnO_2, ZnO), and even multi-component systems (*e.g.*, Au/Pt/ZnO) with robust structural control capabilities.

2 Results and discussion

A large-area (>1 cm^2), uniformly structured monolayer colloidal crystal (MCC) template composed of PS spheres was prepared by a spin-coating process as previously reported (Fig. 1A).[16–20] Considering that the nucleation process during ED is highly dependent on the chemical properties of the material

[a]Department of Engineering Science and Mechanics, The Pennsylvania State University, University Park, PA, 16802 USA. E-mail: szy2@psu.edu; junhuang@psu.edu

[b]Ascent Bio-Nano Technologies Inc., State College, PA, 16801 USA

† Electronic supplementary information (ESI) available: Complete experimental details, additional SEM images, and the assignment of the SERS peaks from the protein and the virus. See DOI: 10.1039/c3tc31635a

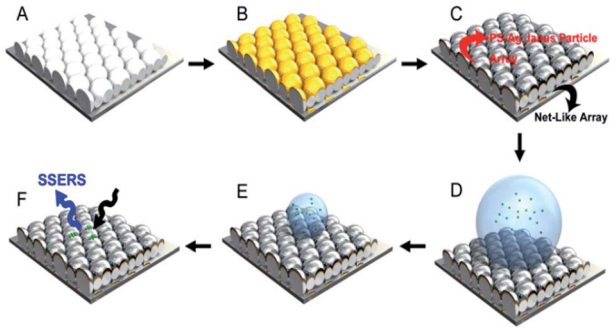

Fig. 1 Schematic demonstration of the site-specific ED growth of the PS–Ag Janus particle array and the net-like array. (A) MCC template. (B) After thermal evaporation of the Au film. (C) Ag was electrodeposited on the Au covered area, giving rise to the formation of the PS–Ag Janus particle array and the net-like array in a single ED growth process. (D) The prepared PS–Ag Janus particle array shows superhydrophobic properties. (E) During water evaporation, concentration of the molecules in the droplet increases. (F) Molecules are delivered to a localized area, facilitating subsequent SERS detection. This concept is called superhydrophobic surface enhanced Raman scattering, or SSERS.

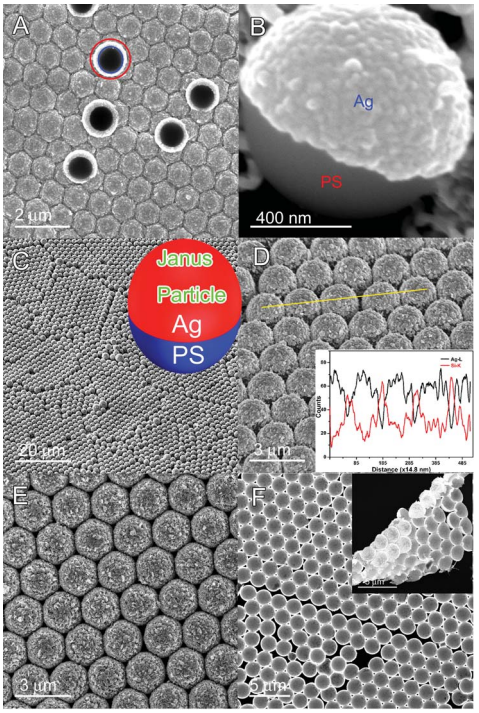

Fig. 2 (A) SEM image of the site-specific ED growth induced PS–Ag Janus particle array. The highlighted circle shows an inverted PS–Ag Janus particle. (B) A single PS–Ag Janus particle. (C) 2 μm diameter PS–Ag Janus particle array. (D) Tilt-view image. Inset: EDS line-scan spectrum. Ag microcup array with openings oriented down (E) and upwards (F). Inset in (F): Ag microcups at the edge area.

interfaces, a 10 nm-thick Au layer was thermally evaporated onto the PS sphere array to provide an appropriate surface. Only the top surface of the PS spheres was covered by the Au film, as the bottom halves of the PS spheres were shielded by shadow effects (Fig. 1B).[18] The MCC template covered by the Au layer was first heated at 110 °C for 10 min to enhance the adhesive force between the PS spheres and the underlying Si substrate, and then used as the cathode to conduct the ED growth of Ag.[9] Details can be found in the ESI (Scheme S1 and Fig. S1†). It was found that Ag was exclusively deposited on the area covered by the pre-deposited Au film (*i.e.*, site-specific growth), resulting in the formation of a hexagonally close-packed PS–Ag Janus particle array and a net-like array (Fig. 1C). The PS–Ag Janus particle array is highly ordered (Fig. 2A), which is inherited from the MCC template. Coverage of Ag on the PS sphere surface is about 50% (Fig. 2B). Because of the different properties of PS and Ag, PS–Ag Janus particle arrays have valuable application potentials in various fields, including self-assembly,[21,22] optics, plasmonics,[23–27] and biomedicine.[28–32] Moreover, PS spheres are commercially available in sizes ranging from 100 nm to more than 10 μm, any of which can be used to create PS–Ag Janus particles to satisfy application demands in broad areas. As an example, an ordered array consisting of 2 μm diameter PS–Ag Janus particles was also prepared (Fig. 2C and D). Line-scan energy dispersive X-ray spectroscopy (EDS) clearly demonstrated that these Janus particles were composed of PS and Ag (inset in Fig. 2D). After dissolving the PS component of the PS–Ag Janus particles using toluene, a well-ordered microcup array was obtained (Fig. 2E). The microcups were inverted by peeling them off from the substrate using an adhesive tape, resulting in a concave-up orientation (Fig. 2F). Observations at the edge area show the curved structure of the Ag microcups (inset in Fig. 2F).

Meanwhile, during thermal evaporation, Au was also deposited on the Si substrate through the gaps within the MCC template, forming a honeycomb array composed of nanotriangles (known as "nanosphere lithography").[33] Similar to the ED growth of Ag on the Au-coated PS spheres, Ag was preferentially deposited on the Au honeycomb array. As Ag deposition proceeded, neighbouring gold nanotriangles in the honeycomb array were gradually bridged (Fig. 3A and B, and insets). By carefully controlling the deposition time, a bow-tie antenna structured Ag surface pattern was obtained (Fig. 3C). Gaps as small as 10 nm between adjacent nanotriangles could be achieved (Fig. 3C). This level of precision, usually inaccessible using traditional lithographical methods, further demonstrates that site-specific ED growth is a robust method for the preparation of surface patterns. The Ag bow-tie surface pattern has significant applications as a plasmonic antenna in particular for SERS sensing applications.[34] After a longer Ag deposition time, a Ag net-like porous film was prepared (Fig. 3D).

In contrast, if a MCC template prepared without the Au seed layer was used as an electrode to perform the ED growth, Ag was exclusively deposited on the Si substrate. After removing the PS spheres, a macro-porous Ag film was fabricated (Fig. S2, ESI†). Therefore, surface properties can indeed influence the nucleation sites during the ED process.

Due to numerous "hot spots" integrated into the highly surface-roughened PS–Ag Janus particles (Fig. 2), the as-prepared PS–Ag Janus particle array demonstrated extremely high SERS sensitivity. Also, it exhibited superhydrophobic

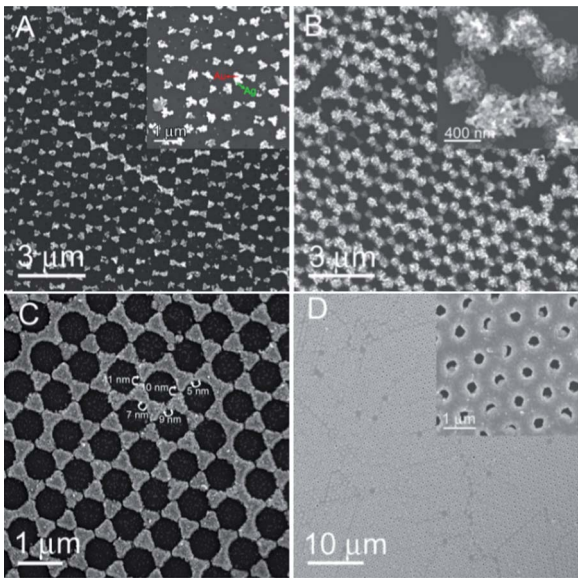

Fig. 3 Selective ED growth of Ag on the Au honeycomb array formed during thermal evaporation. (A), (B), (C), and (D) correspond to deposition times of 1 min, 5 min, 15 min, and 30 min, respectively. Insets in (A), (B), and (D) correspond to zoomed-in images.

properties with a contact angle of about 150° (Fig. 4A and S3 in the ESI†).[35] A microscope image of the PS–Ag Janus particle array is shown in Fig. 4B, displaying an ordered structure. Due to the superhydrophobic properties, when a small amount of an analyte solution was put onto the PS–Ag Janus particle array, a quasi-spherical liquid droplet formed (Fig. 1D). In order to spread the analyte solution on the superhydrophobic PS–Ag Janus particle array to evaluate its SERS performance without employing the superhydrophobic surface-induced enrichment, a small amount (*i.e.*, about 1 wt%) of ethanol was introduced into the Rhodamine 6G (R6G) aqueous solution. Raman spectra of the R6G molecules in aqueous solution at concentrations of 1 nM (curve a) and 1 pM (curve b) are shown in Fig. 4C. Predictably, as evaporation proceeds, the spherical droplet formed by the analyte solution becomes more and more concentrated (Fig. 1E). Eventually, the analyte molecules are delivered to a localized area, immensely facilitating subsequent SERS detection (Fig. 1F). For instance, when 10 μl of the R6G solution with a concentration of 1 fM was applied to the superhydrophobic surface of the PS–Ag Janus particle array, the liquid droplet formed a nearly spherical shape (Fig. 4A).

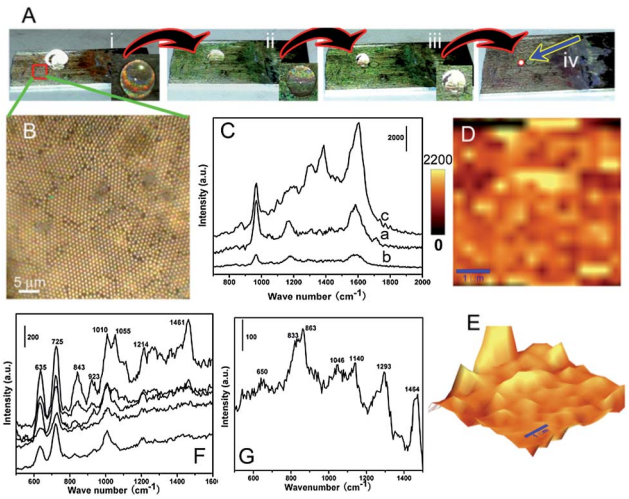

Fig. 4 (A) Experimental results of the superhydrophobic surface-enabled enrichment of analyte molecules. (i) As 10 μl of the R6G solution with a concentration of 1 fM was put onto the PS–Ag Janus particle array. (ii) After solvent evaporation for 50 min, (iii) 70 min, and (iv) 90 min. After 90 min of solvent evaporation, the R6G molecules were delivered to a localized area. (B) Optical image of the SSERS substrate. (C) SERS spectra of R6G. Curves a and b are related to the SERS spectra obtained from R6G solutions with concentrations of 10 nM and 1 pM. Curve c is the SERS spectrum using the SSERS concept with a starting concentration of 1 fM. (D and E) Normal and three-dimensional SERS mapping results of the R6G molecules with an integration time of 1 s. Scale bar in (D) and (E) is 1 μm. (F and G) Raman spectra of 1 nM protein (PV RdRp) and 1 fM virus (poliovirus type I Sabin) acquired by taking advantage of the SSERS concept.

As water evaporated, the volume of the droplet decreased continuously. Simultaneously, the concentration of the R6G in the droplet increased. Evaporation proceeded until the droplet reached a threshold where it became unstable, causing the droplet to collapse and driving the R6G molecules into a localized area (*e.g.*, several tens of square micrometers).[36] Supposing that the diameter of the droplet reaches 10 μm before it becomes unstable and collapses, the concentration of R6G could reach as high as 2×10^{-8} M. Therefore, more than a 10 million-fold enrichment of the molecular concentration can be achieved based on the SSERS concept within 1.5 h.[36] By heating the substrate in an oven maintained at 80 °C, the enrichment process could be reduced to less than 10 min. Experimentally, we realized the SSERS detection of R6G in aqueous solution at a concentration of 1 fM (curve c in Fig. 4C). SERS mapping results verified that an excellent SERS reproducibility was achieved due to the highly ordered structure of the PS–Ag Janus particle array (Fig. 4D and E). Since the PS–Ag Janus particle array could detect R6G solutions with a concentration of 1 pM without taking advantage of the superhydrophobic surface-enabled enrichment effect, theoretically, detection of R6G solutions with initial concentrations as low as 1 attomolar could be anticipated using the SSERS concept.

Proteins are the machinery of life and participate in almost every cellular process. As a proof of concept, we showed the sensitive protein detection of 1 nM of poliovirus (PV) RNA-dependent RNA polymerase (RdRp) (Fig. 4F) using the SSERS substrate. SERS spectra at five randomly chosen sites showed some differences, which were most probably due to the varied protein orientations. Surface modification of the SSERS substrates to anchor protein molecules with the same orientation may solve this problem, which is still under investigation. Low-concentration detection of pathogens is of paramount significance in early-stage disease diagnostics. We further showed low-concentration detection of a virus (PV type I Sabin) of about a 1 fM solution relying on the SSERS concept (Fig. 4G). The origins of the Raman peaks of the PV RdRp protein and the PV type I Sabin can be found in Table S1 and S2 in the ESI.† Further study could achieve ultrasensitive detection of

pathogens and biomarkers using PS–Ag Janus particle arrays relying on the SSERS concept, which has significant importance in early-stage disease diagnostics (*e.g.*, cancer and HIV early-stage diagnostics).

In the following, we demonstrated that the site-specific ED concept could be extended into other material systems, satisfying application demands in diverse fields. Similar to Ag, Cu deposition on PS spheres occurred exclusively on areas first covered with the Au seed layer, leading to the formation of PS–Cu Janus particle arrays (Fig. S4, ESI†). The Cu surface of the PS–Cu Janus particles was composed of many octahedrons, which is a robust example of the potential of seed-assisted site-specific ED growth in preparing Janus particle arrays composed of interesting nanostructures. PS–Cu Janus particles featuring this surface structure have never been reported before.

The structure of the PS–Cu Janus particles can be conveniently controlled by changing the deposition voltage. PS–Cu Janus particles with the Cu face composed of many nanoparticles were prepared by increasing the deposition voltage (Fig. 5A). After removing the PS spheres, hollow Cu hemisphere arrays were prepared (Fig. 5B). A honeycomb array was revealed (Fig. 5C and D) after removing the top-layer hollow hemisphere array. Au nanotriangles were formed by thermal deposition on the substrate through the gaps within the MCC template. Therefore, the PS–Cu Janus particle array and the underlying honeycomb array could be synthesized by a single-step site-specific ED growth.

Multi-component nanomaterials can combine many of the merits of their single-component counterparts, as well as the introduction of unique functionalities. For these reasons, more complex multi-component systems are more attractive in many applications.[37] We further explored the possibility of creating multi-component nanostructured Janus particles using a step-by-step site-specific ED concept. First Pt, and subsequently ZnO were deposited on a 50 nm-thick Au film coated MCC template using ED, resulting in a PS–Au/Pt/ZnO multi-component Janus particle array (Fig. 6A). EDS element-mapping results confirmed that the formation of the multi-component Janus particles formed ordered arrays (Fig. 6D–H). Because of the broad applications of Au and Pt in catalytic areas and ZnO in solar cells and photocatalytic fields,[38] the nest-like PS–Au/Pt/ZnO Janus particle arrays could find applications in diverse fields, with greatly improved performances compared with those of single component nanostructures. Multi-component Janus particles comprised of other materials (*e.g.*, Au/Ag/polyaniline, Au/Pt/SnO_2, Au/Pt/CdS, *etc.*) are also possible using the step-by-step site-specific ED technique.

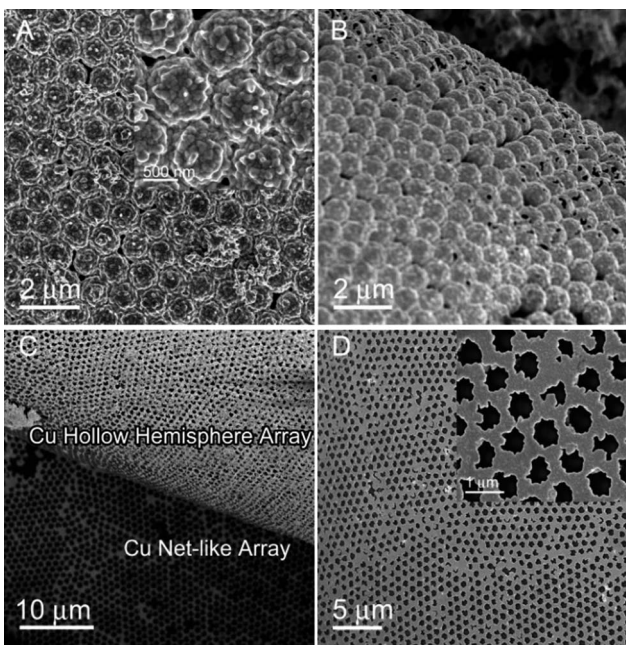

Fig. 5 (A) SEM image of the PS–Cu Janus particle array with Cu surface composed of nanoparticles fabricated at 4 V for 5 min. (B) Hollow Cu hemisphere array after dissolving the PS spheres. (C) Hollow Cu hemisphere array and net-like array formed by a single step seed-layer assisted ED process. (D) Enlarged image of the Cu net-like array.

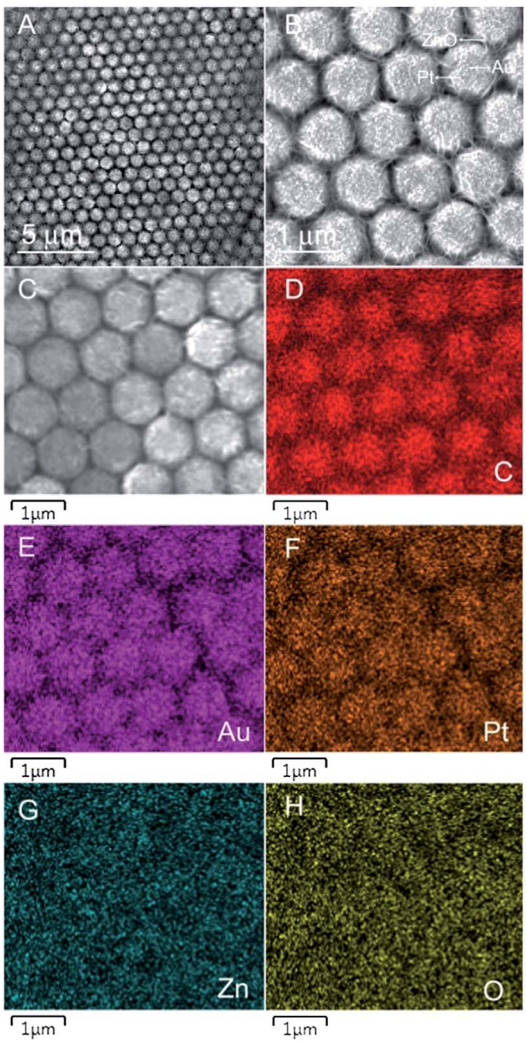

Fig. 6 (A and B) SEM images of the nest-like PS–Au/Pt/ZnO Janus particle array. (C) EDS mapping area. (D–H) EDS element mapping results of C, Au, Pt, Zn, and O, respectively.

At last, the underling mechanism of the site-specific growth has to be discussed, which is helpful for rationally engineering unique nanostructures using the ED method. It is surprising that materials can be electro-deposited on the Au film when it is lacking any obvious physical connection to the electrode (*i.e.*, it is separated from the electrode by the non-conductive PS spheres). Polarization caused by an external electric field induced the contactless ED of polymers and metals on the inner wall surface of a micropore have been reported very recently.[39] The polarization mechanism might contribute to the contactless site-specific ED growth in our case. However, two fundamental questions are waiting to be clarified in the polarization induced contactless ED: where the metal ions get the electrons and how the current flows in the system.[39] Further studies are needed to answer these questions.

Another possibility is that metal ions are first reduced to neutral atoms on the Si substrate, and then some of these atoms aggregate into clusters and grow into gold nanotriangles, resulting in the formation of the bow-tie antenna structured surface patterns (Fig. 3). Other atoms migrate from the Si substrate to the Au film located on the top surface of the PS spheres to form nuclei, subsequently giving rise to the formation of Janus particles (Fig. 2), as shown in Fig. S5 in the ESI.†[40] If this is the case, considering that PS has poor conductivity and Au is a well-known conductor, the nucleation sites during ED are most probably dependent on the conductivity of the substrate. Further investigations about the formation mechanism of the surface patterns through the contactless site-specific ED technique are still needed. A thorough understanding of the mechanism will allow us to rationally design unique, structured surface patterns with strong structural control capabilities.

3 Conclusions

In summary, we have demonstrated that site-specific electrochemical growth was achieved by introducing an appropriate seed layer. Janus particle arrays comprised of metals, metal oxides, and even multi-component materials were prepared, possessing wide applications in self-assembly, solar cells, catalytic areas, sensors, and biomedicine. Over a million-fold enrichment of analyte molecules can be achieved with ease using the superhydrophobic properties of the PS–Ag Janus particle array before SERS detection, enabling an extremely sensitive detection of molecules in a highly diluted solution (*e.g.*, femtomolar level). This SSERS concept is of critical significance in biosensing fields (*e.g.*, ultrasensitive biomarker and pathogen detections).

Acknowledgements

We gratefully acknowledge the financial support from National Institutes of Health (Director's New Innovator Award, 1DP2OD007209-01), National Science Foundation (NSF), the Penn State Center for Nanoscale Science (MRSEC) under grant DMR-0820404, and Huck Innovative & Transformational Seed (HITS) Fund. Components of this work were conducted at the Penn State node of the NSF-funded National Nanotechnology Infrastructure Network.

Notes and references

1 S. Song, Y. Qin, Y. He, Q. Huang, C. Fan and H. Chen, *Chem. Soc. Rev.*, 2010, **39**, 4234–4243.
2 H. S. Cho, E. C. Yeh, R. Sinha, T. A. Laurence, J. P. Bearinger and L. P. Lee, *ACS Nano*, 2012, **6**, 7607–7614.
3 W. C. Law, K. T. Yong, A. Baev and P. N. Prasad, *ACS Nano*, 2011, **5**, 4858–4864.
4 H. J. Han, R. M. Kannan, S. X. Wang, G. Z. Mao, J. P. Kusanovic and R. Romero, *Adv. Funct. Mater.*, 2010, **20**, 409–421.
5 R. A. Alvarez-Puebla and L. M. Liz-Marzan, *Chem. Soc. Rev.*, 2012, **41**, 43–51.
6 M. J. Banholzer, J. E. Millstone, L. D. Qin and C. A. Mirkin, *Chem. Soc. Rev.*, 2008, **37**, 885–897.
7 M. Rycenga, X. H. Xia, C. H. Moran, F. Zhou, D. Qin, Z. Y. Li and Y. Xia, *Angew. Chem., Int. Ed.*, 2011, **50**, 5473–5477.
8 Z. L. Huang, G. W. Meng, Q. Huang, Y. J. Yang, C. H. Zhu and C. L. Tang, *Adv. Mater.*, 2010, **22**, 4136–4139.
9 S. K. Yang, M. I. Lapsley, B. Q. Cao, C. L. Zhao, Y. H. Zhao, Q. Z. Hao, B. Kiraly, J. Scott, W. Z. Li, L. Wang, Y. Lei and T. J. Huang, *Adv. Funct. Mater.*, 2013, **23**, 720–730.
10 S. K. Yang, F. Xu, S. Ostendorp, G. Wilde, H. Zhao and Y. Lei, *Adv. Funct. Mater.*, 2011, **21**, 2446–2455.
11 S. K. Yang, W. P. Cai, L. C. Kong and Y. Lei, *Adv. Funct. Mater.*, 2010, **20**, 2527–2533.
12 X. Chen, Y. Wu, B. Su, J. Wang, Y. Song and L. Jiang, *Adv. Mater.*, 2012, **24**, 5884–5889.
13 K. S. Liu, X. Yao and L. Jiang, *Chem. Soc. Rev.*, 2010, **39**, 3240–3255.
14 Y. Li, T. Sasaki, Y. Shimizu and N. Koshizaki, *J. Am. Chem. Soc.*, 2008, **130**, 14755–14762.
15 T. S. Wong, S. H. Kang, S. K. Y. Tang, E. J. Smythe, B. D. Hatton, A. Grinthal and J. Aizenberg, *Nature*, 2011, **477**, 443–447.
16 X. Ye and L. Qi, *Nano Today*, 2011, **6**, 608–631.
17 N. Vogel, J. Fischer, R. Mohammadi, M. Retsch, H. Butt, K. Landfester, C. K. Weiss and M. Kreiter, *Nano Lett.*, 2011, **11**, 446–454.
18 M. C. Gwinner, E. Koroknay, L. Fu, P. Patoka, W. Kandulski, M. Giersig and H. Giessen, *Small*, 2009, **5**, 400–406.
19 S. K. Yang, W. P. Cai, J. L. Yang and H. B. Zeng, *Langmuir*, 2009, **25**, 8287–8291.
20 S. K. Yang and Y. Lei, *Nanoscale*, 2011, **3**, 2768–2782.
21 J. Yan, M. Bloom, S. C. Bae, E. Luijten and S. Granick, *Nature*, 2012, **491**, 578–582.
22 Q. Chen, J. K. Whitmer, S. Jiang, S. C. Bae, E. Luijten and S. Granick, *Science*, 2011, **333**, 199–202.
23 Y. Liu, Q. Hao, J. S. T. Smalley, J. Liou, I. C. Khoo and T. J. Huang, *Appl. Phys. Lett.*, 2010, **97**, 09101–09103.
24 B. Zhang, Y. Zhao, Q. Hao, B. Kiraly, I. C. Khoo, S. Chen and T. J. Huang, *Opt. Express*, 2011, **19**, 15221–15228.
25 B. K. Juluri, Y. Zheng, D. Ahmed, L. Jensen and T. J. Huang, *J. Phys. Chem. C*, 2008, **112**, 7309–7317.

26 Y. Zhao, S. C. S. Lin, A. A. Nawaz, B. Kiraly, Q. Hao, Y. Liu and T. J. Huang, *Opt. Express*, 2010, **18**, 23458–23465.
27 Y. Zheng, T. J. Huang, A. Y. Desai, S. J. Wang, L. K. Tan, H. Gao and A. C. H. Huan, *Appl. Phys. Lett.*, 2007, **90**, 183117–183119.
28 S. Yang, F. Guo, B. Kiraly, X. Mao, M. Lu, K. W. Leong and T. J. Huang, *Lab Chip*, 2012, **12**, 2097–2102.
29 X. Mao and T. J. Huang, *Lab Chip*, 2012, **12**, 1412–1416.
30 W. Gao, A. Pei, X. Feng, C. Hennessy and J. Wang, *J. Am. Chem. Soc.*, 2013, **135**, 998–1001.
31 Q. Chen, J. Yan, J. Zhang, S. C. Bae and S. Granick, *Langmuir*, 2012, **28**, 13555–13561.
32 Q. Chen, J. K. Whitmer, S. Jiang, S. C. Bae, E. Luijten and S. Granick, *Science*, 2011, **331**, 199–202.
33 N. Vogel, M. Jung, N. L. Bocchio, M. Retsch, M. Kreiter and I. Koper, *Small*, 2010, **6**, 104–109.
34 K. D. Ko, A. Kumar, K. H. Fung, R. Ambekar, G. Liu, N. Fang and K. C. Toussaint, *Nano Lett.*, 2011, **11**, 61–65.
35 The superhydrophobic property was induced by the micro/nanostructured Ag surface of the PS–Ag Janus particles. If the gold seed layer was wrapped around the entire PS sphere surface, PS–Ag core–shell structures formed the array as expected, which should also have superhydrophobic properties and can be used as a SSERS substrate.
36 F. D. Angelis, F. Gentile, F. Mecarini, G. Das, M. Moretti, P. Candeloro, M. L. Coluccio, G. Cojoc, A. Accardo, C. Liberale, R. P. Zaccaria, G. Perozziello, L. Tirinato, A. Toma, G. Cuda, R. Cingolani and E. Di Fabrizio, *Nat. Photonics*, 2011, **5**, 682–687.
37 L. Qu, R. A. Vaia and L. Dai, *ACS Nano*, 2011, **5**, 994–1002.
38 E. S. Jang, J. H. Won, S. J. Hwang and J. H. Choy, *Adv. Mater.*, 2006, **18**, 3309–3312.
39 A. Bouchet, E. Descamps, P. Mailley, T. Livache, F. Chatelain and V. Haguet, *Small*, 2009, **5**, 2297–2303.
40 J. Ustarroz, J. A. Hammons, T. Altantzis, A. Hubin, S. Bals and H. Terryn, *J. Am. Chem. Soc.*, 2013, **135**, 11550–11561.